J. Membrane Biol. 197, 49–58 (2004)
DOI: 10.1007/s00232-003-0641-z

The Journal of
Membrane
Biology

Distributions-per-Level: A Means of Testing Level Detectors and Models of Patch-Clamp Data

I. Schröder[1], T. Huth[1], V. Suitchmezian[1], J. Jarosik,[2] S. Schnell[1], U.P. Hansen[1]
[1]Center of Biochemistry and Molecular Biology, Leibnizstr. 11, 24098 Kiel, Germany
[2]Bioenergetics Institute, Adam Mickiewicz University, Poznan, Poland

Received: 11 July 2003/Revised: 22 October 2003

Abstract. Level or jump detectors generate the reconstructed time series from a noisy record of patch-clamp current. The reconstructed time series is used to create dwell-time histograms for the kinetic analysis of the Markov model of the investigated ion channel. It is shown here that some additional lines in the software of such a detector can provide a powerful new means of patch-clamp analysis. For each current level that can be recognized by the detector, an array is declared. The new software assigns every data point of the original time series to the array that belongs to the actual state of the detector. From the data sets in these arrays distributions-per-level are generated. Simulated and experimental time series analyzed by Hinkley detectors are used to demonstrate the benefits of these distributions-per-level. First, they can serve as a test of the reliability of jump and level detectors. Second, they can reveal beta distributions as resulting from fast gating that would usually be hidden in the overall amplitude histogram. Probably the most valuable feature is that the malfunctions of the Hinkley detectors turn out to depend on the Markov model of the ion channel. Thus, the errors revealed by the distributions-per-level can be used to distinguish between different putative Markov models of the measured time series.

Key words: Amplitude histograms — Beta distributions — Discrimination of models — Hinkley detector — Markov models — Noise — Sublevels

Correspondence to: U.P. Hansen; email: uphansen@zbm.uni-kiel.de

Abbreviations: AMFE = anomalous mole fraction effect; C, Z = closed state; DHD = sublevel Hinkley detector; HMM = Hidden Markov model; O, F = open state; S = subconductance level.

Introduction

The kinetic behavior of ion channels is described by Markov models (Korn & Horn, 1988; Yeo et al., 1988; Ball & Rice, 1992; Blunck et al., 1998). There are three methods for revealing an adequate Markov model and for evaluating the rate constants of the transitions between the states of these Markov models: 1. Applying level and jump detectors in order to create dwell-time histograms (Schultze & Draber, 1993; Colquhoun, Hatton & Srodzinsky, 1996; Blunck et al., 1998). 2. Applying a direct fit to the time series using a Maximum Likelihood estimator (Fredkin & Rice, 1992; Albertsen & Hansen, 1994; Klein, Timmer & Honerkamp, 1997; Farokhi, Keunecker & Hansen, 2000; Hansen et al., 2003) 3. Creating amplitude histograms and fitting the deviations from Gaussians by beta distributions (FitzHugh, 1983; Yellen, 1984; Klieber & Gradmann, 1993; Riessner, 1998).

Dwell-time analysis requires reliable detectors for estimating the current levels of the time series and for detecting the jumps (times of the transitions from one conducting state to another). The direct fit of the time series needs only a level detector, whereas beta distributions can be generated without any detector. Farokhi, Keunecke and Hansen (2000) have shown that the direct fit of the time series is more powerful than dwell-time analysis at the edge of temporal resolution. Nevertheless, dwell-time analysis is much less time-consuming; analysis and results are more obvious to the researcher, whereas the HMM fit works in the dark tunnel of mathematics, as it does not provide a graphical control of the procedure. The output is just some numbers (rate constants), which the researcher has to believe. Thus, there is still a role for dwell-time analysis (Colquhoun, Hatton & Hawkes, 2003) and consequently a need for reliable jump detectors. The investigations reported here will

show that the analysis of beta distributions, too, can profit from level and jump detection.

Noise and fast gating often lead to malfunctions of the employed detectors. Every jump detector has an integration time to smooth out noise. Increasing this integration time reduces false alarms (fake transitions induced by noise), but increases the number of missed events. Schultze and Draber (1993) employed simulated time series to find an optimum compromise between false alarms and missed events with Hinkley detectors.

More desirable than transferring the settings of the detector (integration time) from simulated data to experimental data would be a test that can reveal the malfunctions of the detectors. Here, the analysis of distributions-per-level is introduced. Distributions-per-level can be obtained by adding a simple routine to the software of the detectors. The additional software compares the measured time series with the reconstructed one as obtained from the employed level and/or jump detector. It opens one data array per detected current level; all data points from the measured time series are assigned to these arrays as suggested by the actual level indicated by the detector. From these arrays, amplitude histograms are created resulting in distributions-per-level.

For the investigations below, Hinkley detectors (Schulze & Draber, 1993; Draber & Schulze, 1994b) are employed, because they are a little bit faster than low-pass filters with threshold detectors (because real integration replaces low-pass filtering, and an algorithm deleting trends in the "wrong" direction keeps the detector alert). The investigation of the performance of the distributions-per-level showed their ability to estimate malfunctions of the detectors. However, more interestingly, they provided some fringe benefits, namely a means of discriminating different Markov models suggested for the measured time series. Another benefit enhancing the power of beta distribution analysis in order to get a quantitative description of fast gating, is illustrated for experimental data.

Materials and Methods

Electrophysiological Measurements

Patch-clamp measurements were performed on cytosolic droplets of *Chara* as described previously (Farokhi et al., 2000; Hansen et al., 2003) or on Maxi-K channels (Moss & Magleby, 2001; Shi & Cui, 2001) expressed in HEK cells (a gift from Prof. U. Seydel and Dr. A. Schromm, Research Center, Borstel). For *Chara* droplets, the pipette (luminal) was filled with 250 mM KNO_3 + 5 mM $Ca(NO_3)_2$ and the bathing medium (cytosolic) contained 230 mM KNO_3 + 20 mM $TlNO_3$ + 5 mM $Ca(NO_3)_2$. For HEK cells, the solution in the pipette (luminal) was in mM. 5 KNO_3, 140 $NaNO_3$, 1.2 $Mg(NO_3)_2$, 4.17 $NaHCO_3$, 0.44 KH_2PO_4, 0.34 Na_2HPO_4, pH = 7.2, and in the bathing medium (cytosolic) it was 10 TlCl, 140 KCl, 5 $MgCl_2$, 10 HEPES, pH = 7.2.

The experimental setup is described in detail by Draber and Hansen (1994). Briefly, electrodes were made from borosilicate glass (Hilgenberg, Malsfeld, Germany) coated internally with Sigmacote (Sigma, Deisenhofen, Germany), drawn on an L/M-3P-A puller (List, Darmstadt, Germany), and filled with the solution mentioned above. External coating with Sylgard (Dow Corning, USA) was not employed. Instead, the technique of Keunecke (Farokhi et al., 2000) of keeping the pipette with the excised patch (inside-out) close to the surface of the bathing solution (20 μm) reduced noise to a σ of less than 1 pA at 50 kHz bandwidth. Patch-clamp current was recorded by a Dagan 3900A amplifier (Dagan, Minneapolis, Minnesota, USA) with a 4-pole anti-aliasing filter of 50 kHz. Data was stored on disk with a sampling rate of 200 kHz.

Simulation of Surrogate Time Series

Time series were generated from a selected Markov model with an assumed set of states and rate constants. As described in detail previously (Blunck et al., 1998; Caliebe, Rösler & Hansen, 2002; Riessner et al., 2002), a temporal sequence of sojourns in the states of the assumed Markov model was generated, and the true single-channel current assigned to the actual state was superimposed by white noise as defined by the selected signal-to-noise ratio (SNR). The resulting signal was fed into the same filter as used for the filtering of the experimental data (program available at http://www.zbm.uni-kiel.de/software).

Generating Distributions-per-Level

Our patch-clamp program for data analysis (kielpatch.exe on http://www.zbm.uni-kiel.de/software) includes three built-in Hinkley detectors: First-Order Hinkley Detector, Higher-Order (8^{th}) Hinkley Detector (HOHD, Schulze & Draber, 1993) and the Dynamic Hinkley Detector (DHD, Draber & Schulze, 1994b) that can also detect sublevels. The Hinkley detectors need a-priori information, i.e., the putative current levels and the related variance in order to get optimum settings of the threshold for jump detection (Schultze & Draber, 1993). The levels can be supplied by three different methods: a) fit of the amplitude distributions by a sum of Gaussians; b) fit-by-eye and c) automatic level detector. Riessner et al. (2002) have shown that fit-by-eye and the automatic detector perform equally well, whereas the analysis of the amplitude histogram by Gaussian distributions fails in noisy time series with fast gating.

Distributions-per-level were obtained from a bookkeeping routine added to the software of the Dynamic Hinkley detector (DHD). This routine creates different data arrays, one for each current level. The routine sorts the data points of the measured time series into that array indicated by the actual level as suggested by the Hinkley detector.

Modeling and Experimental Results

Test of Detectors

If a detector works well, the distributions-per-level of a time series without fast gating should be Gaussian distributions around the nominal current values. However, missed events and false alarms (Schultze & Draber, 1993) spoil this nice picture. The suggested test of the performance of the detector is illustrated by means of surrogate data, i.e., by time series sim-

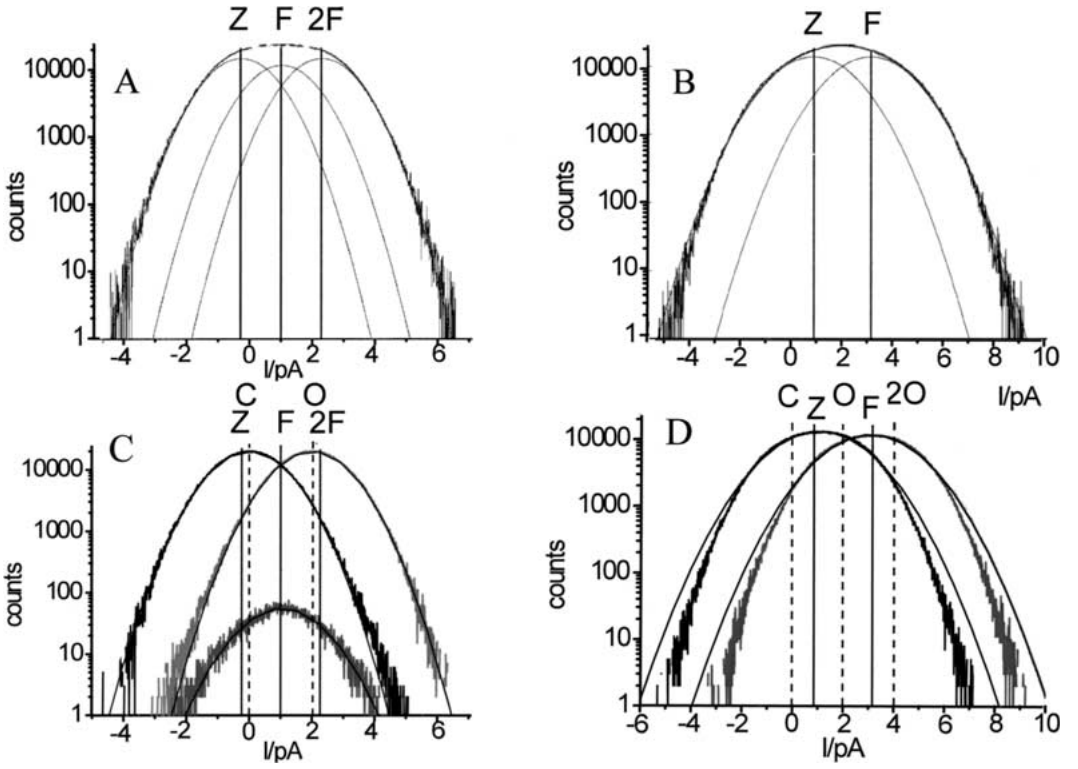

Fig. 1. Distributions-per level as a means of detecting malfunctions of the level detectors. (*A*) Time series simulated from a symmetrical C-O model with the rate-constants $k_{CO} = k_{OC} = k = 1000\ s^{-1}$. Current of the open state is 2 pA and the noise variance is $\sigma = 1$ pA. The amplitude histogram is fitted by a two-channel model with the states *Z* (closed), *F* (one channel open) and 2*F* (two channels open). The fit yields the following currents: $I(Z) = -0.24$ pA, $I(F) = 1$ pA and $I(2F) = 2.37$ pA. The variance was smaller than that of the simulation, $\sigma = 0.92$ pA. The parameters obtained from this fit are used as settings for the Hinkley detector, resulting in distributions-per-level shown in (*C*). The resulting two major distribution functions can be fitted with their peaks located at 0 and 2 pA and $\sigma = 1$ pA, i.e., exactly the values used for the simulation of (*A*). (*B*) Here, a two-channel model ($2 \times C$-*O*) with nominal currents at 0 pA, 2 pA and 4 pA and $\sigma = 1.2$ pA is fitted by a simple *Z*-*F* model resulting in $I(Z) = 0.85$ pA, $I(F) = 3.16$ pA and $\sigma = 1.43$ pA. (*D*) Distributions-per-level obtained from the two-state fit of (*B*) with levels at 0.85 pA and at 3.1 pA with $\sigma = 1.64$ pA.

ulated from an assumed Markov model as described above.

The models used for illustrating the performance of the distributions-per-level are quite simple models with one state for each conductance level. Hidden Markov Models (HMM) are not employed because level detectors do not recognize jumps between states of equal conductivity (kinetic states that are not distinguished by the applied experimental procedure can be merged into apparent states, Hansen, Tittor & Gradmann, 1983).

Figure 1*A* shows the amplitude histogram obtained from a *C*-*O* model (one open state *O* and one closed state *C*) with the parameters given in the legend. Because of high noise, the individual peaks cannot be distinguished. This amplitude histogram should be fitted by the sum of two Gaussians (*not shown*), but a good fit is also obtained with a sum of three Gaussians (shown by the Gaussians in Fig. 1*A*). The fit with this wrong Scenario is quite perfect and supports the statement by Riessner et al. (2002) that the fit of amplitude histograms is the least reliable means of determining current levels. Thus, the experimenter erroneously believes that the time series can be fitted with three levels, with the currents and variance taken from the Gaussians in Fig. 1*A*. The DHD detector with the settings from the three Gaussians finds sojourns at the assumed levels. These levels (*Z*, *F*, 2*F*) are given as solid vertical lines in Fig. 1*C*, whereas the true levels *O* and *C* are denoted by dotted lines.

The distributions-per-level in Fig. 1*C* delivered by the Hinkley detector show two important features (with *O*, *C* being the true levels, *Z*, *F*, 2*F* those found by the detector).

1. The distributions related to *Z* and 2*F* peak at the true levels *C* and *O* (Fig. 1*C*). This indicates that *Z* and 2*F* were the wrong choice.
2. The distribution related to *F* has its peak at level *F*. This may be unexpected as we know that there is no level *F*. Here an effect may come into play that is investigated in more detail below, namely the generation of sublevels by the anti-aliasing filter of the recording apparatus. The filter smoothes the transitions between currents levels, generating data

points between the levels. Further, noise may locate some adjacent data points in the range of the detector looking at level *F*.

Nevertheless, the deviations of the peaks of the two major distributions clearly indicate that the detector was set to the wrong levels, thus revealing the incorrect hypothesis. In addition, the peaks of these distributions indicate the location of the true levels.

The other way round does not work so well, i.e., generating the time series with a three-state model (*C-O-2O*) and analyzing it erroneously with a two-state model. Figure 1*B* shows that a perfect fit of the amplitude histogram can be obtained with two Gaussians at level *Z* and *F*. Using these parameters as settings for the DHD yields the distributions-per-level in Fig. 1*D*. The two distributions look quite good. The only indication of malfunction is the feature that the top is broader than the basis. If the distributions are fitted with Gaussians (smooth lines in Fig. 1*D*) then most of the data points close to the peak determine the parameters of the fit. Figure 1*D* shows that at the base the fitted distribution is wider than the experimentally determined one. This is unusual, as in all cases investigated below, the base tends to be wider than the top (relative to the Gaussian distribution). Nevertheless, this is quite a weak argument for rejecting the incorrect fit of Fig. 1*B*. There are two better approaches. The first one is to look for a jump-free section of the time series. Then it becomes obvious that the noise of the fitted distributions is higher than that of the jump-free section. The second approach would be an attempt to make a fit with a higher number of levels. If the number of estimated levels is higher than that of the measured time series, this would be indicated by a phenomenon such as that in Fig. 1*C*.

In the following sections, additional indications of malfunctions are obtained and discussed. However, a probably more important feature of the distributions-per-level will be demonstrated: discrimination between different Markov models and investigation of the origin of sublevels.

Model Discrimination

Forbidden Transitions

The kinetic behavior of channel gating is described by Markov models. Often it is difficult to make a decision as to whether a putative model is the correct one. Here some examples are given that show that the distributions-per-level can be helpful. However, it is not possible to distinguish between states of equal conductivity in Hidden Markov models.

The first case deals with the problem addressed previously by Caliebe et al. (2002) and Draber and Schultze (1994a). Two scenarios are compared: Scenario 2Ch ("two channel"): two identical channels with three levels: *C* (closed), *S* (sublevel) and *O* (open). Scenario 4Ch ("four channel"): A set of four channels, two with the levels *C* and *S* and two with the levels *C* and *O*.

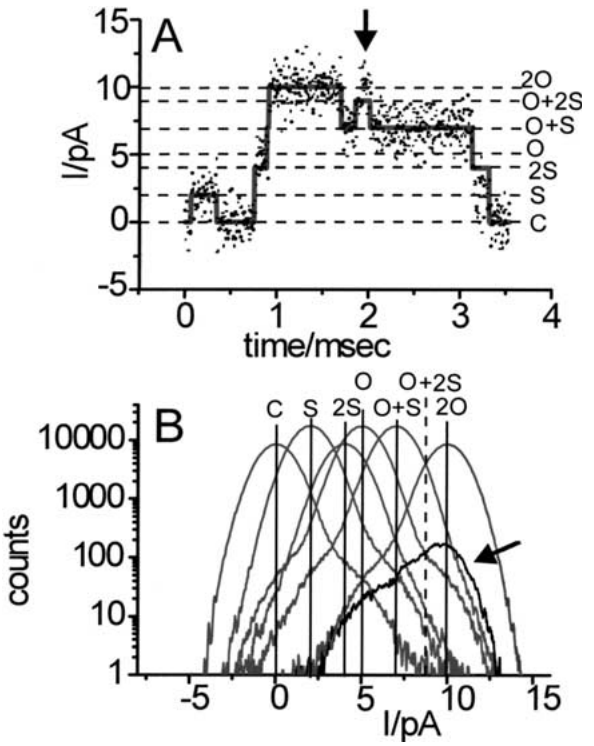

Fig. 2. Time series generated by scenario 2Ch (2 cyclic *C-S-O*-models as in the inset of Fig. 4*B*, *C*) with all rate constants = 1000 s^{-1} and current in $S = 2$ pA and in $O = 5$ pA, variance of the noise $\sigma = 1$ pA. (*A*) Section of the time series showing the incorrect operation of the Hinkley detector adapted to the wrong model (scenario 4Ch). (*B*) Distributions-per-level created from the time series in (*A*).

A time series is generated on the basis of scenario 2Ch, i.e., 2 channels *C-S-O*. However, the researcher does not know the correct scenario. Imagine that the DHD (Draber & Schultze, 1994b) is set erroneously to analyze the time series on the basis of the wrong scenario 4Ch. The DHD Hinkley detectors search and find events on all levels of the scenario 4Ch, i.e., C, S, $2S$, O, $O+S$, $O+2S$, $2O$, $2O+S$, $2O+2S$. Thus, seeing only the record of the Hinkley detector (Fig. 2*A*) and the related dwell-time distributions (*not shown*), the experimenter is tempted to believe that scenario 4Ch (2 small and 2 big channels) holds. (Even though $2O+S$ and $2O+2S$ have not been observed, the experimenter may believe that these levels occur too rarely.) Now, the generation of the distributions-per-level helps to detect a wrong choice of model. Fig. 2*B* shows that the "false" levels do not peak at their nominal current values but at a current level that occurs only in (the correct) scenario 2Ch. This shows that the Hinkley detector has done in-

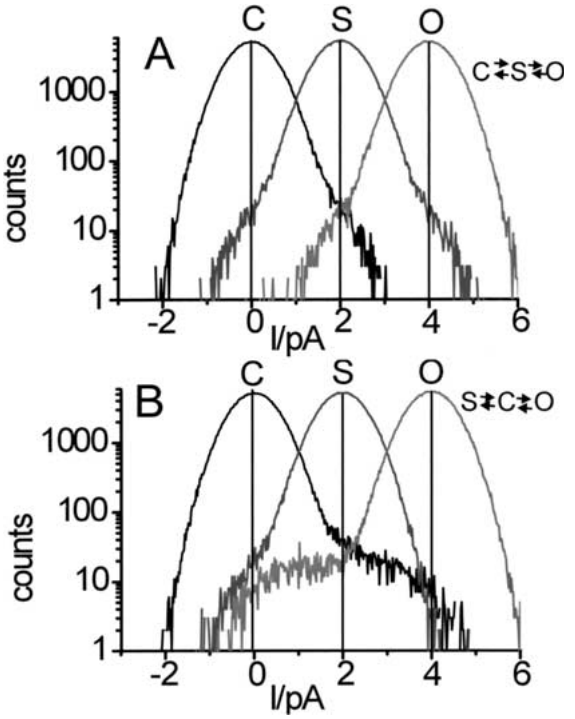

Fig. 3. Revealing the sequence of states. (*A*) Distributions-per-level obtained from a time series simulated for a *C-S-O* model with the following settings: all rate constants 1000 s^{-1}, current in $S = 2$ pA, current in $O = 4$ pA, variance of the noise $\sigma = 1$ pA. (*B*). Distributions-per-level obtained from a time series simulated for an *S-C-O* model with the same currents and rate constants.

correct assignments. An example of such an incorrect assignment is shown by the arrow in Fig. 2*A*. The channel has jumped to level 2*O*, but that one of the simultaneously working Hinkley detectors aiming at $O+2S$ has won the race (Draber & Schultze, 1994a). The Hinkley detector thus claims to have seen level $O+2S$. The distributions-per-level, however, show that $O+2S$ is not an allowed level, as it does not peak at its nominal value in Fig. 2*B*. The peak at 2*O* indicates that the detector erroneously has taken jumps to 2*O* as jumps to $O+2S$, as shown in Fig. 2*A*.

Sequence of Levels

The second case deals with the sequence of levels. Time series are generated for two different scenarios, and it is tested whether the distributions per level can tell which one of the two models was used to generate the investigated time series. Scenario *CSO* consists of one channel with the Markov model *C-S-O*. The Markov model of scenario *SCO* is *S-C-O*. Thus, the only difference between the two scenarios is the order of states. Time series were generated for both scenarios with the rate constants given in the legend of Fig. 3. The Hinkley detector (DHD, Draber & Schultze, 1994b) uses the same settings for both scenarios: it looks for the levels C, S, and O.

Figure 3 shows that the distributions-per-level can find out which time series belongs to which scenario. The crucial feature that becomes obvious in Fig. 3 is obtained from the comparison of the right-hand slopes of the *S*-level-distributions in Fig. 3*A* and Fig. 3*B*. This slope shows a perfect Gaussian shape in Fig. 3*B*, but not in Fig. 3*A*. The reason is obvious: the transition *O*-*S* must not occur in scenario *SCO* in Fig. 3*B*, and levels *O* and *S* are never adjacent. Thus, the detector cannot erroneously remain in *S* when the channel has already jumped into state *O*, because such a transition does not occur. This criterion corresponds to that of the transition matrices suggested by Draber and Schultze (1994b). On the other hand, the bulge on the right-hand side of the *C*-level distribution extending to level *O* indicates that the channel has already jumped from *C* to *O*, but the detector has failed to realize this. The same holds for the left-hand side of the *O*-level distribution. The origin of the bulges on the slopes of the distributions in Fig. 3*B* lies in the fact that the detector has failed to realize in time the jump from *C* to *O*, or missed events have occurred, i.e., jumps into state *O* that have not been realized by the detector.

Cyclic vs. Linear Markov Models

The third case shows that cyclic models can be distinguished from linear models. Scenario CYC is a cyclic model as shown in the inset of Fig. 4*B*/*C*. Scenario LIN is a linear model as shown in the inset of Fig. 4*D*/*E*.

Time series were generated for both models with the rate constants as given in the legend of Fig. 4. Figures 4*B* and *D* reveal a feature that is already known from Fig. 3: In the model *S-C-O* (Fig. 4*D*) the transition between *S* and *O* must not occur. This is indicated by the Gaussian slope on the right-hand side of the distribution of level *S*. The bulge on the left-hand side of *O* may be considered as an example against this argument. However, the long extension of the bulge indicates that it results from undetected $O \rightarrow C$ jumps, similar to the right-hand bulge of the *C*-level distribution resulting from $C \rightarrow O$ jumps.

Thus, it is already possible to distinguish between scenario CYC and scenario LIN on the basis of the criterion applied in Fig. 3: Deviations from the Gaussian slope indicate that a transition may occur. (This means that the sleepiness of the detector helps to reveal existent transitions).

However, there is another test. The software of the Hinkley detector provides the option to forbid certain transitions. The distributions-per-level in Fig. 4*C* and Fig. 4*E* are obtained under the constraint that the transitions between *S* and *O* are forbidden. This constraint should not affect scenario LIN, because this transition must not occur. Basically, the distributions in Fig. 4*D* and *E* look very similar. The only

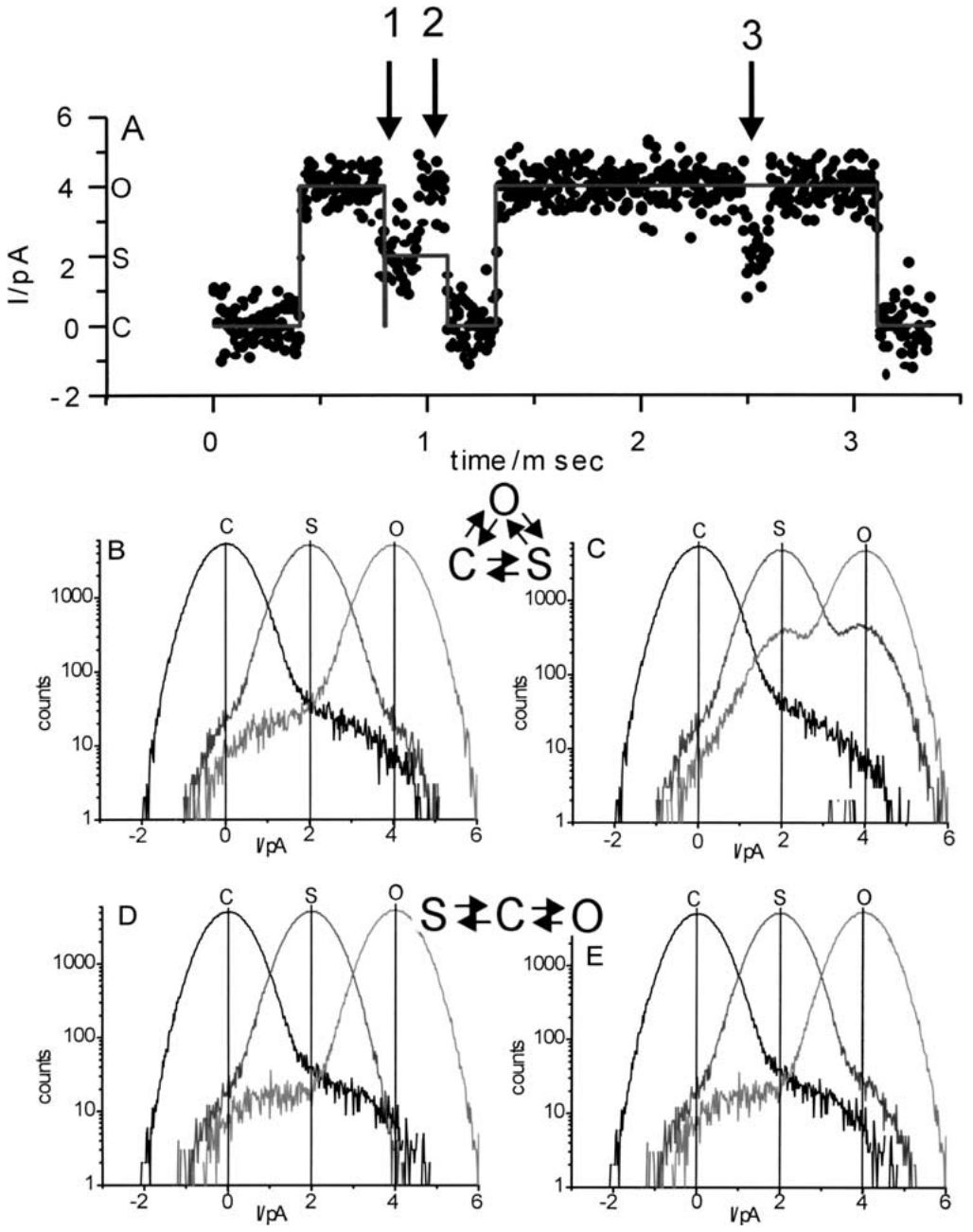

Fig. 4. Distributions-per-level obtained with and without restriction for the Hinkley detector from time-series generated from two different models, as indicated by the insets. (*A*) Simulated time series obtained from the cyclic model of (*B*) and (*C*). The solid line gives the reconstructed time series provided by the Hinkley detector. Arrows indicate malfunctions. (*B*, *C*) Cyclic model with all the rate constants being 1000 s^{-1}. (*D*, *E*) Linear Markov model with all the rate constants being 1000 s^{-1}. (*C*) and (*E*): Distributions-per-level from level detectors working under the constraint that the transitions *S*-*O* are forbidden.

difference is that in Fig. 4*E* a bulge also occurs on the right-hand side of the *S*-distribution. This is difficult to understand. A solution may be as follows. If there are jumps $S \rightarrow C \rightarrow O$, and the sojourn in *C* is not realized by the detector (or if a double jump has occurred), then a jump $S \rightarrow O$ seems to have occurred in the experimental data. If the detector is fast enough this rare event would not spoil the slope in Fig. 4*E*. However, if the transition $S \rightarrow O$ is forbidden, then the detector remains in the nominal level *S*, but the data points belong to *O*.

Thus, the introduction of the restriction inactivates the criterion of Fig. 3, but a better criterion is obtained instead: now, the distributions of level *S* and *O* in Fig. 4*C* display satellite peaks at the wrong levels. In the cyclic model, transitions between *O* and *S* do occur, but the detector is not allowed to follow them.

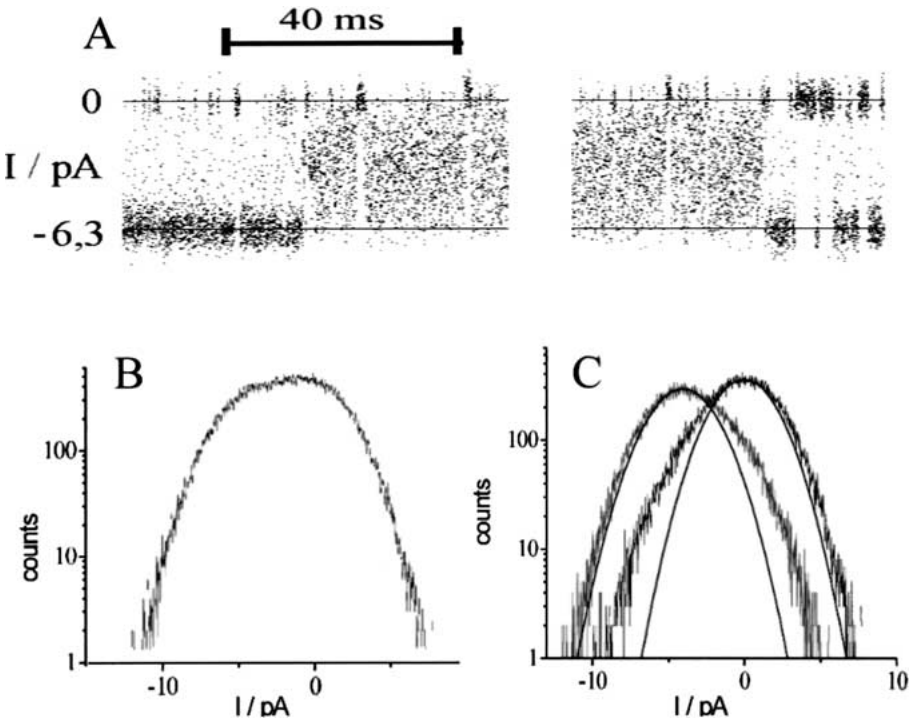

Fig. 5. Revealing beta distributions as caused by fast gating by means of the distributions-per-level. (*A*) Time series obtained from a Maxi-K channel expressed in HEK-cells showing mode switching, i.e., a sudden change in the kinetic properties of the channel (the middle part of about 150 ms has been omitted in order to show the transitions with higher temporal resolution). (*B*) Overall amplitude histogram of the middle section of (*A*) showing fast flickering. (*C*) Distributions-per-level. The smooth lines give the Gaussian distribution of the noise as obtained from the section of the time series with slow gating (right- and left-hand side of *A*).

Examples are shown in Fig. 4*A*. At arrow *1*, the time series jumps from *O* to *S*. The detector, however, can jump to *S* only via the allowed transitions *O*-*C*-*S*. This may occur also with restriction, and consequently the extensions of the *C*-distributions into the range of the *S* and *O* distributions is of the same magnitude in Fig. 4*B* and Fig. 4*C*. The interesting events occur at arrow *2* and arrow *3*. At arrow *2*, the time series jumps from *S* to *O*, but the detector is not allowed to follow. Thus, data points of *O* are assigned to level *S*, leading to the satellite peak of the *S*-distribution at level *O* in Fig. 4*C*. The situation at arrow *3* in Fig. 4*A* gives an example of the generation of the satellite peak of the *O*-distribution at level *S* in Fig. 4*C*.

The situations indicated by arrows *2* and *3* do not occur in the *S*-*C*-*O* model. The restriction has an effect only if double jumps occur. However, they are rare. Nevertheless, they may lead to the small difference between Fig. 4*D* and *E* discussed above.

Revealing Fast Gating

The detection of fast gating in a measured time series is still a difficult problem. Farokhi et al. (2000) have shown that dwell-time analysis fails near the corner frequency of the anti-aliasing filter. The direct fit of the time series with a Hidden-Markov model can extend the range to higher rate constants (and thus was successful in detecting the fast gating causing the reduction of the apparent single-channel current in the AMFE; Farokhi et al., 2000; Hansen et al., 2003). However, an even more powerful means is the analysis of beta distributions describing the gating-induced deviation of the amplitude histogram from the Gaussian distribution caused by the noise of the jump-free time-series (FitzHugh, 1983; Yellen, 1984; Klieber & Gradmann, 1993; Riessner, 1998). The generation of Beta distributions by fast gating is illustrated in Fig. 6, below. In experimental data, the beta distributions of individual levels may be hidden in the sum of the distributions of all levels.

Here we show that the distributions-per-level may be helpful. Figure 5*A* shows a time series obtained from a Maxi-K channel under conditions given in Materials and Methods. After a long record with moderate switching, all of a sudden the channel enters a mode of fast gating. At the right-hand side of Fig. 5*A*, it returns to the original mode. This time series clearly demonstrates how fast gating leads to a reduction of apparent single-channel current. In Fig. 5*A*, the effect is immediately obvious. This is similar to the situation of the Cs^+ block of the K^+ channel in *Chara* (Draber & Hansen, 1994), whereas in the case of the K^+/Tl^+ AMFE in *Chara* the reduction of apparent single-channel current by fast gating had to be revealed by means of a long mathematical analysis (Farokhi et al., 2000).

The interval of fast flickering in Fig. 5*A* is used for the generation of the distributions in Fig. 5*B* and *C*. Figure 5*B* gives the overall-amplitude distribution. It is obvious that details cannot be recognized. However, the distributions-per-level in Fig. 5*C* clearly show the occurrence of beta distributions. The distribution of the closed state is asymmetrical and the *O*-distribution has become broader than the distri-

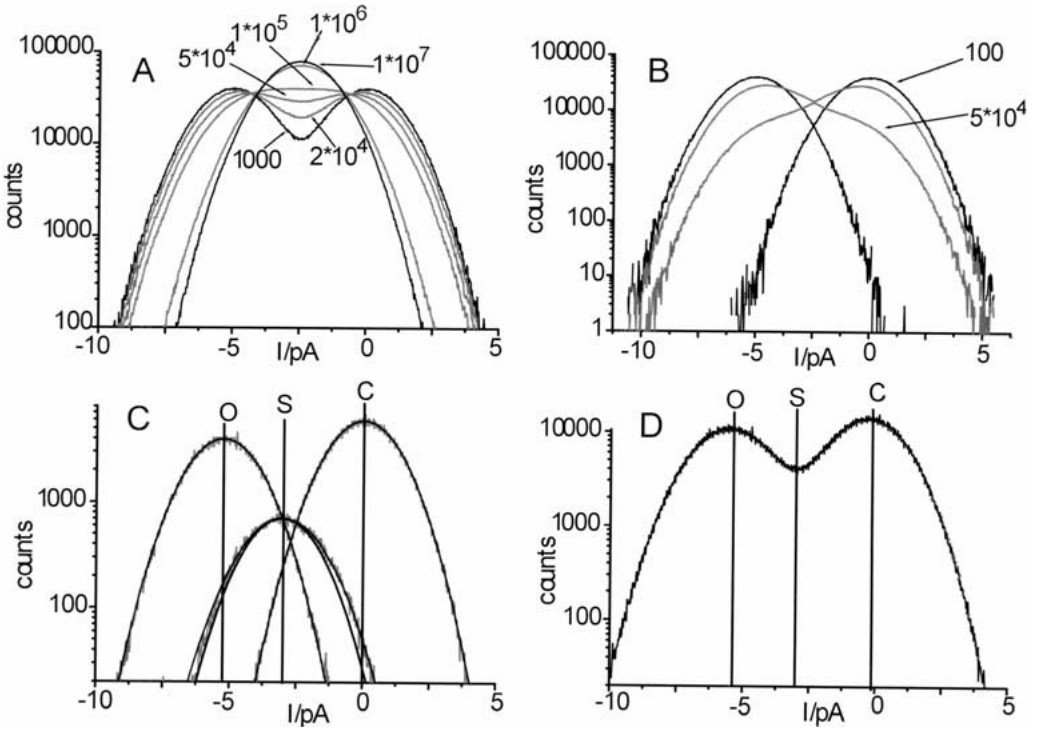

Fig. 6. Comparison of sublevels generated by fast flickering in surrogate data and those measured in inside-out recordings from the dominant K^+ channel in the tonoplast of *Chara*. Simulated and real data with $I(O) = -5$ pA, noise $\sigma = 1$ pA, bandwidth of 4-pole Bessel filter = 50 kHz. (*A*) Simulated data in a symmetrical C-O model with the rate constants $k_{CO} = k_{OC} = k$ as given on the curves in s^{-1}. (*B*) Distributions-per-level at $k = 50{,}000\ s^{-1}$ and at $k = 100\ s^{-1}$. (*C*) Distributions-per-level obtained from *Chara*. (*D*) The overall amplitude histogram from *Chara*.

bution of apparent jump-free sections of the time series (smooth lines in Fig. 5*C*).

Here, the data from the Maxi-K channel serve to demonstrate the new approach opened by the distributions-per level. The detailed analysis of the beta distributions in Fig. 6 is carried out in the framework of the investigation of the occurrence of the K^+/Tl^+-AMFE in Maxi-K channels and will be published in a forthcoming paper.

Sublevels and Fast Gating

In our experiments on the K^+ channel in *Chara*, there were times when sublevels occured very frequently, and at other times they did not occur for months. There were two questions that could not be settled. 1. What conditions caused their appearance? 2. Were they true conductance levels, or were they just apparent levels as caused by averaging over fast gating? We do not see how to tackle the first question, but the distributions-per-level may provide a means of solving the second question. If the sublevels arise from fast gating, distributions-per-level may reveal beta distributions as in the example of Fig. 5.

In order to study what kinds of effect can occur, fast flickering producing an apparent sublevel was generated by an *O-C* model. A two-state model is sufficient, because longer sojourns in the *C*- and *O*-state do not contribute to the putative flickering causing the sublevel.

Figure 6*A* shows distributions resulting from a fast flickering *O-C* model. The rate-constants k_{OC} and k_{CO} are equal. This is to be expected because the sublevel has been found to occur in the middle between *C* and *O*. Figure 6*B* gives an estimate in what range of rate constants the generation of a sublevel by fast flickering can occur and what effects on the shape of the distributions-per-level are to be expected.

The curves in Fig. 6*A* show that there is a limited range of rate constants where the distribution functions would reveal gating as the origin of the sublevels. If the rate constants are too slow (up to $k =$ filter bandwidth), analysis would identify the two original levels *O* and *C*. If they are too fast ($10^7\ s^{-1}$), the filter smoothes out the effects of gating, and the beta distribution does not get wider than the Gaussian distribution of the superimposed noise.

The curves in Fig. 6*A* are compared with that one obtained from the sublevel (*S*) of the measured data in Fig. 6*C*. Since these sublevels are in the middle between *O* and *C*, the putative rate constants of the flickering have to be symmetrical. This implies that there is no skewing of the beta distributions as in the *C*-level distribution in Fig. 5. The only candidate for

indicating fast gating is the width of the beta distribution. Unfortunately, the distribution of the sublevel in *Chara* is only 10% broader than that of the Gaussian distribution of the noise of a jump-free time series (inner smooth line in the middle distribution of Fig. 6*C*). In Fig. 6*A* 10% broadening is obtained for $k = 10^6$ s^{-1}. No sign of this broadening can be observed in the overall amplitude histogram of Fig. 6*D*.

It may be questioned whether the broadening of the sublevel distribution in Fig. 6*C* really results from fast gating (beta distribution) or whether it originates from a malfunction of the detector. However, the message that can be taken from Fig. 6*C* is that the broadening is not more than 10%. This implies that if these sublevels originate from fast gating the rate constants must be higher than 10^6 s^{-1}. This means that for a current of 6 pA of the full level on average only 40 ions can pass the pore during one mean open time.

Fig. 6*C* thus gives an estimation of how fast a recording system has to be in order to test whether sublevels are caused by fast gating.

Discussion

Usually, level detectors work hidden in an encapsulated sphere of mathematics. There are few and not very efficient statistical means of controlling their operation by means of simulations (Schulze & Draber, 1993; Riessner et al., 2002). The determination of the distributions-per-level turns out to provide a look into this dark sphere and watch the performance of the level detectors. The integrals over the bulges in Fig. 3 may provide an estimate of how many data points were assigned to the wrong levels.

However, distributions-per-level may not only act as supervisors of level detectors (Figs. 1 and 2); the ability to distinguish between different Markov models as shown in Figs. 2 to 4 may become a useful means of modelling.

Revealing beta distributions, as in Figs. 5 and 6, would be a very important means of increasing temporal resolution if the distributions-per-level obtained by the extended software of the Hinkley detector are reliable. As shown in Figs. 1 to 4, deviations from the Gaussian form may be caused by malfunction of the Hinkley detector. However, the comparison of Figs. 1 to 4 with Figs. 5 and 6 shows that the beta distributions have a more harmonic curve shape than those resulting from the failures of the detector. This strengthens the belief that the observed beta distributions are true.

A general theory is not yet available, but simulations can help. It has to be recommended that every statement obtained from this kind of analysis has to be tested on surrogate data. Simulations have to be employed in order to check whether the model obtained from the analysis generates exactly the time series and distribution functions that have been obtained directly from the data. In a second step, alternative models have to be used for the generation of the simulated time series and to check whether the related distributions differ significantly from those of the measured data. This would be an indication of how unique the evaluated model is.

Even if the distributions-per-level do not result in an unambiguous conclusion it provides an additional and powerful criterion for testing hypotheses by simulations. If this interplay between surrogate and experimental data is done thoroughly, the distributions-per-level can turn out to be a useful means of model discrimination and of increasing temporal resolution.

This work was supported by the Deutsche Forschungsgemeinschaft. We are grateful to Prof. Dr. J. Dainty, Norwich, UK, for critical reading and to Prof. Dr. U. Seydel and Dr. A. Schromm for the gift of HEK cells expressing Maxi-K channels.

References

Albertsen, A., Hansen, U.P. 1994. Estimation of kinetic rate constants from multi-channel recordings by a direct fit of the time series. *Biophys. J.* **67:**1393–1403

Ball, F.G., Rice, J.A. 1992. Stochastic models for ion channels: introduction and bibliography. *Math. Biosci.* **112:**189–206

Blunck, R., Kirst, U., Rießner, T., Hansen, U.P. 1998. How powerful is the dwell-time analysis of multi-channel records? *J. Membrane Biol.* **165:**19–35

Caliebe, A., Rösler, U., Hansen, U.P. 2002. A χ^2 test for model determination and sublevel detection in ion channel analysis. *J. Membrane Biol.* **185:**25–41

Colquhoun, D., Hatton, C.J., Hawkes, A.G., 2003. The quality of maximum likelihood estimates of ion channel rate constants. *J. Physiol.* **547:**699–728

Colquhoun, D., Hawkes, A.G., Srodzinski, K. 1996. Joint distributions of apparent open times and shut times of single ion channels and the maximum likelihood fitting of mechanisms. *Phil. Trans. R. Soc. Lond.* A **354:**2555–2590

Draber, S., Hansen, U.P. 1994. Fast single-channel measurements resolve the blocking effect of Cs^+ on the K^+ channel. *Biophys. J.* **67:**120–129

Draber, S., Schultze, R. 1994a. Correction for missed events based on a realistic model of a detector. *Biophys. J.* **66:**191–202

Draber, S., Schultze, R. 1994b. Detection of jumps in single-channel data containing subconductance levels. *Biophys. J.* **67:**1404–1413

Farokhi, A., Keunecke, M., Hansen, U.P. 2000. The Anomalous Mole Fraction Effect in *Chara*: Gating at the edge of temporal resolution. *Biophys. J.* **79:**3072–3082

Fredkin, D.R., Rice, J.A. 1992. Maximum likelihood estimation and identification directly from single-channel recordings. *Proc. Roy. Soc. Lond.* B **249:**125–132

FitzHugh, R. 1983. Statistical properties of the asymmetric random telegraph signal with application to single channel analysis. *Mathematical Bioscience* **64:**75–89

Hansen, U.P., Cakan, O., Abshagen, M., Farokhi, A. 2003. Gating models of the Anomalous Mole Fraction Effect of single-channel current in *Chara*. *J. Membrane Biol.* **192:**45–63

Hansen, U.P., Tittor, J., Gradmann, D. 1983. Interpretation of current-voltage relationships for "active" ion transport systems: II. Nonsteady-state reaction kinetic analysis of class I mechanisms with one slow time-constant. *J. Membrane Biol.* **75:**141–169

Klein, S., Timmer, J., Honerkamp, J. 1997. Analysis of multi channel patch clamp recordings by Hidden Markov models. *Biometrics* **53:**870–884

Klieber, H.G., Gradmann, D. 1993. Enzyme kinetics of the prime K^+ channel in the tonoplast of *Chara*: selectivity and inhibition. *J. Membrane Biol.* **132:**253–265

Korn, S.J., Horn, R. 1988. Statistical discrimination of fractal and Markov models of single-channel gating. *Biophys. J.* **54:**871–877

Moss, B.L., Magleby, K.L. 2001. Gating and conductance properties of BK channels are modulated by the S9-S10 tail domain of the α subunit. A study of mSlol and mSlo3 wild-type and chimeric channels. *J. Gen. Physiol.* **118:**711–734

Riessner, T. 1998. Level Detection and Extended Beta Distributions for the Analysis of Fast Rate Constants of Markov Processes in Sampled Data. PhD thesis, Kiel, Germany and Shaker-Verlag, Aachen.

Riessner, T., Woelk, F., Abshagen, M., Hansen, U.P. 2002. A new level detector for ion channel analysis. *J. Membrane Biol.* **189:** 105–118

Schultze, R., Draber, S. 1993. A nonlinear filter algorithm for detection of jumps in patch-clamp data. *J. Membrane Biol.* **132:** 41–52

Shi, J., Cui, J. 2001. Intracellular Mg^{2+} enhances the function of BK-type Ca^{2+}-activated K^+ channel. *J. Gen. Physiol.* **118:**589–605

Yellen, G. 1984. Ionic permeation and blockade in Ca^{2+} activated K^+ channels of bovine chromaffin cells. *J. Gen. Physiol.* **84:** 157–186

Yeo, G.F., Milne, R.K., Edeson, R.O., Madsen, B.W. 1988. Stastistical inference from single channel records: two state Markov model with limited time resolution. *Proc. R. Soc. Lond.* B **235:**63–94